Borehole Breakout Numerical Modelling for In-Situ Stress Estimation

Kutay E. Karadeniz and H. Ozturk

Abstract**—** In-situ stress is one of the important rock properties used in different engineering disciplines; there are some techniques applied to determine in-situ stresses. One of them is borehole breakouts to estimate both orientation and magnitudes, carried out in drill holes; they are formed by induced stress exceeding compressive strength of rock around borehole wall. In this paper, estimation of in-situ horizontal stress magnitudes from borehole breakout geometries was studied in terms of depth of breakouts measured from center of borehole. The borehole cross sections were mimicked in FLAC numerical modelling software to establish a relation between ratio of breakout depth to borehole radius and stress magnitudes for given maximum horizontal stress. Then, these were compared with the field data for the back-analysis of numerical solutions. The purpose is obtaining an empirical equation of maximum horizontal stress in terms of breakout depth, borehole radius, compressive strength and minimum horizontal stress for the field studied.

Keywords**—** Borehole Breakout, Breakout Depth, Horizontal Stresses, Numerical Analysis

I. Introduction

Breakouts are stress-induced compressive borehole failures that cause cross-sectional change in borehole wall and represent spalled zones predicted on opposite sides of the boreholes in the minimum horizontal principal stress (S_{hmin}) direction [1, 2]. After drilling a borehole, if magnitudes of the stresses exceed the compressive strength (C_0) of rock, the sections, on the minimum horizontal stress direction, might be spalled [3-8]. Therefore, breakouts are considered important indicators for the estimation of the minimum stress direction orthogonal to the axis of the borehole. They are also sufficient to specify the maximum stress orientation (S_{hmax}) by adding 90 degrees to the direction estimated in case there is no drilling induced fracture (DIF) data. DIFs are stress induced tensile fractures at the azimuth of S_{hmax} as an indicator of S_{hmax} orientation as well in breakouts for S_{hmin}. The magnitudes and the directions of these stresses might be derived by the corresponding shapes of these breakouts in terms of width (W_{BO}) and depth (r_d) [8].

In some researches, the Mohr-Coulomb failure criterion was applied to the stress distribution for a circular section to compare the stresses in the borehole surface; these studies have shown that the breakouts are caused by compressive shear failures, resulting in that they are appeared to be "dog ear shaped", where fractures are formed near the borehole wall [2, 7]. Zoback *et al.* [7] have studied the breakout mechanism, the elastic stresses that exceed the strength of the rock, using Mohr-Coulomb shear failure criterion; the created flat-bottomed failure zones were stated to be the initial breakout zones. Nevertheless, Mastin [9] developed a numerical model to analyze breakout growth; this study concluded that the formed spalled region of breakout may be extended in advance of S_{hmin} direction as breakout depth (r_d) after initial state of growth. Besides the extension in depth, it was stated that information of C_0, magnitude of S_{hmin} and W_{BO} are sufficient to estimate magnitude of S_{hmax} since circumferential stresses around the borehole diminishes soon after the initial failure of breakout formation; this results in stop widening of breakouts [10]. Hence, the use of W_{BO} and r_d might differ in estimation of S_{hmax}.

In this study, borehole breakout geometry in terms of depth was studied to express a relation between r_d and varying S_{hmax} by numerical analysis using FLAC software for given C_0, S_{hmin} and other rock properties cohesion (S_0), internal friction angle (φ), elastic modulus (E) and Poisson's ratio (ν). The output of the numerical analyses were compared with the field data acquired from the borehole imaging tool, Formation Micro Imager (FMI). Moreover, the results of the analytical and the numerical analysis were also compared in terms of using W_{BO} and r_d and the difference in the estimation of the magnitude of S_{hmax}.

II. FMI Log – Data Acquisition

To obtain breakouts and DIFs along a borehole, borehole imaging tools are required, in that way, information in terms of number, azimuth, breakout depth and width, and depth in a borehole could be gathered. Different imaging tools are used to provide images of borehole surfaces; these tools depend on distinctive physical properties, such as resistivity, acoustics, optical and density image logs; although they are generally used as resistivity and acoustic imaging tools. While acoustic imaging tools utilize measures of acoustic wave travel time and reflected amplitude in many directions at any depth, resistivity imaging tools create images of the surfaces using resistivity contrast [11].

FMI depends on four-arm calipers in aspect of working principle; they both have four arms with mounted resistivity pads. It provides two outputs in borehole analysis; these are resistivity images measuring the conductivity difference transmitting current and caliper logs measuring the distance between opposite pads of the four arms.

Kutay. E. Karadeniz is in the Middle East Technical University, Ankara, Turkey, Department of Mining Engineering, Ankara, Turkey,

H. Ozturk is in the Middle East Technical University, Department of Mining Engineering, Ankara, Turkey,

https://doi.org/10.17758/EARES7.EAP0819203

In resistivity images, dark regions refer to high conductivity zones with lower resistivity readings of the pads; those zones demonstrate that there is a rock breakage. The rock breakage might be breakouts, DIFs, or any other failure type such as washout and key-seat. To differentiate which one of these occur, some conditions must be checked to answer the description of the failures. DIFs might be controlled by the interpretation of the resistivity image in aspect of orthogonality of those fractures, parallel to the borehole axis; they must exist at opposite sides of the borehole surface. In detection of breakouts, they might be misinterpreted with washouts and key-seats; caliper logs and resistivity images of FMIs are both required to define the extent of failure at the same time. In other words, they have to be observed together with caliper logs giving the cross-sectional shape change instantaneously moving along the entire borehole and in resistivity image giving the opposite dark zones. Caliper logs have two lines corresponding to the measured distance between conjugate pad pairs. If there is no extension in borehole perimeters, both lines coincide. One of the lines separate from the other one, this means that there is a spalled zone in the borehole surface causing enlargement in the perimeter. Thus, analyzing both the image and caliper logs are required for the identification of breakouts [6].

In this study, the borehole analyzed with FMI has 8 breakouts with different azimuths, breakout depths (r_d), and widths (W_{BO}), varying 40^0 to 50^0, and there is no DIFs along the entire borehole obtained. In the previous study, the orientations of S_{hmax} and S_{hmin} were estimated as N11.25W and N78.75E, respectively for the same borehole. [12]

III. Analytical and Numerical Analyses

The numerical modelling software FLAC, was used in this study to analyze breakout dimension under various S_{hmax} combinations. It uses an explicit finite difference code for 2D analysis of different geotechnical problems, such as rock, soil, ground support, etc. The 2D borehole section was analyzed at a constant S_{hmin} with different S_{hmax} combinations in plane strain condition. As mentioned before, the results of FLAC 2D were compared with the analytical results for the given rock strength parameters and the S_{hmin} magnitude.

A. *Analytical Analysis*

The effective maximum and minimum principal stresses due to stress concentration resulting from the removed material that cannot be supported by field stresses are given by Kirsch equations [13] and by Jaeger and Cook [14]. Tangential and radial effective stresses in Equation 1, 2, 3 are defined in terms of S_{hmax}, S_{hmin}, radius of the borehole (R), distance from the center of the borehole (r), azimuth measured from the direction of S_{hmax} (θ), and the difference between the mud weight in the borehole and the pore pressure (ΔP).

$$\sigma_{rr} = \frac{1}{2}(S_{hmax} + S_{hmin})(1 - \frac{R^2}{r^2}) + \frac{1}{2}(S_{hmax} - S_{hmin})(1 - 4\frac{R^2}{r^2} + 3\frac{R^4}{r^4})\cos 2\theta + \frac{\Delta P R^2}{r^2} \quad (1)$$

$$\sigma_{\theta\theta} = \frac{1}{2}(S_{hmax} + S_{hmin})(1 + \frac{R^2}{r^2}) - \frac{1}{2}(S_{hmax} - S_{hmin})(1 + 3\frac{R^4}{r^4})\cos 2\theta - \frac{\Delta P R^2}{r^2} \quad (2)$$

$$\tau_{r\theta} = -\frac{1}{2}(S_{hmax} + S_{hmin})(1 + \frac{2R^2}{r^2} - 3\frac{R^4}{r^4})\sin 2\theta \quad (3)$$

According to Equation 1 and 2, the effective stresses change as a function of azimuth and distance from the center of the borehole. Pore pressure, mud weight, and correspondingly ΔP are not covered in this study. Therefore, in case the pressure is equal to zero and r is equal to R for the stresses at the boundary of the borehole with plane strain condition can be expressed using Equation 4 and 5 where θ is 90° and 0°, respectively.

$$\sigma_{\theta\theta} = 3S_{hmax} - S_{hmin} \quad (4)$$

$$\sigma_{\theta\theta} = 3S_{hmin} - S_{hmax} \quad (5)$$

With the assumption that the tangential stress is equal to C_0, S_{hmax} can be found by substituting the magnitude of S_{hmin} and an azimuth (θ) of 90° into Equation 2. The magnitude of the S_{hmin} was obtained by the leak-off test carried out on site and resulted as 3.5 MPa. Leak-off test is one of the pressure integrity tests used for the purpose of finding the minimum formation pressure or S_{hmin}. After the laboratory strength tests were conducted, C_0 was determined as 27.6 MPa. Thus, the S_{hmax} can be estimated analytically as 10.4 MPa.

In addition to the analytical results, depending on Kirsch equations, Barton *et al.* [10] stated that a relation exists to determine S_{hmax} by the knowledge of rock strength and W_{BO} since W_{BO} value does not change during the process of breakout growth. The reason of this stable condition is the stress concentration in equilibrium with the strength of the rock at the edge of a breakout [15]. In this way, the Equation 6 can be used to estimate S_{hmax};

$$S_{hmax} = \frac{(C_0 + \Delta P + 2P)}{(1 - 2\cos 2\theta_b)} - S_{hmin}\frac{(1 + 2\cos 2\theta_b)}{(1 - 2\cos 2\theta_b)} \quad (6)$$

In Equation 6, θ_b is the angle between the azimuth of S_{hmax} and the edge of a breakout initiated. If the half width of a breakout is defined as angle ϕ_b, the relation between these two measures can be represented by Equation 7.

$$\phi_b = \frac{\pi}{2} - \theta_b \quad (7)$$

It is found out that W_{BO} changes between 40° and 50°, correspondingly, and ϕ_b varies between 20° and 25°. Therefore, S_{hmax} was calculated as a range by the substitution of θ_b, ranging between 65° to 70°. In addition to the variation in W_{BO} with identical parameters; C_0 and S_{hmin} were determined as 27.6 MPa and 3.5 MPa, respectively and neglected ΔP and P (pore pressure) as indicated in Kirsch equations, the estimated S_{hmax} was found to be in the range of 11.6 MPa and 12.5 MPa.

B. *Input Parameters of Numerical Analysis*

Laboratory strength tests to determine uniaxial and triaxial compression strength and indirect tensile strength were conducted to identify the mechanical properties of intact rock samples taken from the field as seen in Table I.

TABLE I: THE MECHANICAL PROPERTIES OF THE ROCK USED IN FLAC

Properties	Value
Poisson's Ratio	0.23
Young's Modulus	7.18 GPa
Density	2.1 g/cm^3
Cohesion	6.82 MPa
Internal Friction Angle	32.6°
Dilation Angle	0°
Tensile Strength	5.2 MPa

As stated by Zheng *et al*. [8], radial stresses cause increasing confinement in the regions away from the borehole boundaries, failure is more likely to occur as shear fracture; therefore, using these parameters, FLAC models were run with Mohr-Coulomb failure criterion. Furthermore, perfectly-plastic material behavior was assigned to the model based on the stress-strain curves of the laboratory experiments.

C. Numerical Analysis Results

In the numerical analysis, a full square domain with empty circular section representing a borehole in the center is assigned in the model. The rectangular section is not fixed; S_{hmax} and S_{hmin} are applied orthogonally to all boundaries instead, see Fig. 1. In other words, the far field stresses are applied to the model as the boundary conditions. This model was run in both elastic and plastic states; hence the validation was done comparing the results of elastic run and the analytical solutions, Equations 1,2, and 3, in terms of variation of radial and tangential stresses as a function of the distance from borehole boundaries to far field. By this model, a vertical borehole was modeled in plane strain condition to analyze failure modes with different stress magnitudes in aspects of change in depth of formed breakouts.

Fig 1. Modelling Geometry with S_{hmax} and S_{hmin}

In this way, increase in depth of borehole breakouts was obtained by the model with a radius of 0.108 m. With the given parameters and the failure criterion, while the S_{hmin} estimated by leak-off tests was kept constant, the magnitude of the S_{hmax} was gradually increased by 0.5 MPa increments in each run. Until the S_{hmax} magnitude reached 10.5 MPa, no failure occurred along the perimeter of the borehole. However, dog-ear shaped borehole breakouts were observed after a certain level of S_{hmax}. These 25 runs were carried out up to 22 MPa of S_{hmax}. The yielded elements due to compressive shear failure are represented by yellow and red zones, see Fig. 2.

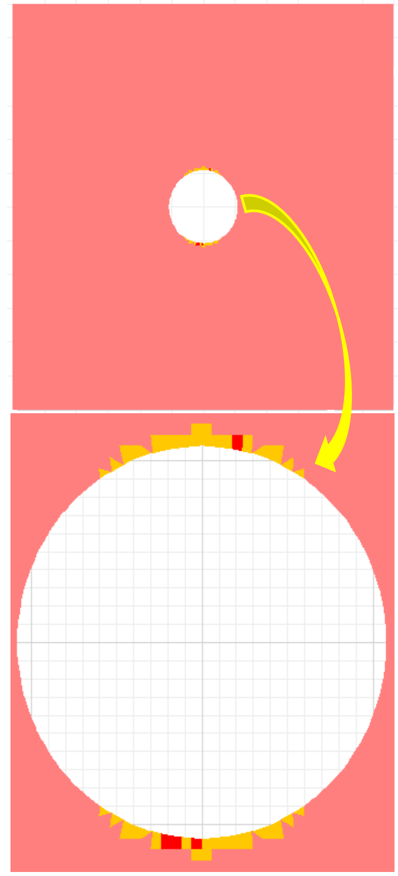

Fig 2. Representative Model Geometry with Yielded Elements

The values of breakout depths and their normalized depths are summarized in Table II; the normalized breakout depth represents the change as a percentage of the borehole radius.

The results of the models listed in Table II, were used to establish a relation between breakout dimensions as the depth and the given stress - strength magnitudes. The tangential stresses or so called "hoop stresses" [15] can be calculated by elastic theory mentioned by the Equation 1,2, and 3; besides, the objective is the estimation of S_{hmax} by the correlation created using r_d, S_{hmin}, and C_0 of the field.

Fig. 3 shows the relation of normalized breakout depth and the ratio of maximum hoop stresses (as given in Equation 4) to C_0; thus, the y-axis of the graph is normalized breakout depth as percentage and x-axis gives the equation of stress-strength ratio [16]. Since the variation and the numerical accuracy caused some limitations for the numerical analysis by the software, there are two more curves in addition to the average trendline, including upper and lower limits of the results obtained. In this way, this provides a range of magnitude of S_{hmax} for a given borehole breakout depth.

TABLE II: MODELING RESULTS

S_{hmax} (MPa)	S_{hmin} (MPa)	r_d (m)	Normalized Breakout Depth (% of r)
10	3.5	0.1080	0.0000
10.5	3.5	0.1143	5.8795
11	3.5	0.1145	6.0035
11.5	3.5	0.1151	6.5440
12	3.5	0.1161	7.5065
12.5	3.5	0.1228	13.6929
13	3.5	0.1233	14.1650
13.5	3.5	0.1238	14.6312
14	3.5	0.1244	15.1739
14.5	3.5	0.1253	16.0418
15	3.5	0.1296	19.9657
15.5	3.5	0.1308	21.1476
16	3.5	0.1312	21.4959
16.5	3.5	0.1321	22.3005
17	3.5	0.1322	22.4484
17.5	3.5	0.1394	29.0992
18	3.5	0.1399	29.5127
18.5	3.5	0.1399	29.5485
19	3.5	0.1406	30.1642
19.5	3.5	0.1474	36.4839
20	3.5	0.1495	38.4607
20.5	3.5	0.1498	38.6878
21	3.5	0.1508	39.6595
21.5	3.5	0.1512	39.9778
22	3.5	0.1514	40.1778

The best fit curves of average, upper, and lower limits are expressed as in Equations 8,9, and 10, respectively.

$$S_{hmax} = \frac{\left(e^{2.10\frac{r_d}{r}-2.123}\right)C_0 + S_{hmin}}{3} \tag{8}$$

$$S_{hmax} = \frac{\left(e^{2.11\frac{r_d}{r}-2.164}\right)C_0 + S_{hmin}}{3} \tag{9}$$

$$S_{hmax} = \frac{\left(e^{2.10\frac{r_d}{r}-2.087}\right)C_0 + S_{hmin}}{3} \tag{10}$$

In Table III, breakout depths, the normalized breakout depths and their corresponding S_{hmax} magnitudes of the field data from the best fit curves are given.

TABLE III: FIELD DATA

r_d (m)	Normalized Breakout Depth (% of r)	Average Curve S_{hmax}	Upper Limit S_{hmax}	Lower Limit S_{hmax}
0.1343	24.44	16.22	15.77	16.84
0.1257	16.67	13.95	13.56	14.47
0.1223	13.33	13.08	12.72	13.57
0.1415	31.11	18.48	17.97	19.20
0.1331	23.33	15.87	15.43	16.47
0.1403	22.22	15.53	15.10	16.12
0.1223	30.00	18.08	17.58	18.78

IV. CONCLUSION

The objectives of this study are the introduction of a methodology to estimate the S_{hmax} by borehole breakout with its depth and the comparison of the results obtained from the analytical and the numerical analyses. By this study, there were different S_{hmax} magnitudes acquired; S_{hmax} is equal to 10.4 MPa by Kirsch equations [13], and it is in the range of 11.6 MPa and 12.5 MPa according to Barton *et al.* [10]. However, the best fit curves from numerical modelling indicate S_{hmax} magnitudes of 12.7 MPa to 19.2 MPa.

The following conclusions have been achieved based on the performed analyses:

- FLAC models might lead to underestimation of the breakout depths, in other words, it might result in fewer yielded elements compared to the actual case on field. The reason for this might be explained by incapability of FLAC for the modelling of fracture propagation using fracture toughness properties of the material.
- Time dependency in borehole breakout growth is crucial, time dependent crack growth is claimed to depend on subcritical crack growth [8]. It is considered that there are some reasons resulting in these subcritical cracks in rocks; these are stress corrosion, dissolution, diffusion, and microplasticity etc. [17]. It is also proposed that breakout growth is strongly correlated with chemical and hydrologic conditions. Furthermore, absorption of strain energy through inelastic deformation may also cause time dependent failure after the rock failure begins. After breakouts are initiated, although their widths stay stable, they have a tendency to deepen [15].

These implications might be the reasons of differences in the results from the three approaches covered in this study. Therefore, this study has provided a range for the S_{hmax} magnitude in estimation within a certain accuracy.

REFERENCES

[1] Gough, D. I., & Bell, J. S. (1981). Stress orientations from oil-well fractures in Alberta and Texas. Canadian Journal of Earth Sciences, 18(3), 638-645. https://doi.org/10.1139/e81-056

[2] Bell, J. S. and Gough, D. I. (1983). The use of borehole breakouts in the study of crustal stress, in Hydraulic fracturing stress measurements. D.C, National Academy Press, Washington.

[3] Cox, J. W. (1970, January). The high resolution

dipmeter reveals dip-related borehole and formation characteristics. In SPWLA 11th Annual Logging Symposium. Society of Petrophysicists and Well-Log Analysts. https://doi.org/10.2118/72-01-02
[4] Bell, J. S., & Gough, D. I. (1979). Northeast-southwest compressive stress in Alberta evidence from oil wells. Earth and planetary science letters, 45(2), 475-482. https://doi.org/10.1016/0012-821X(79)90146-8
[5] Hickman, S. H., Healy, J. H., Zoback, M. D., Svitek, J. F., & Bretches, J. E. (1982). In-situ stress, borehole elongation, and natural fracture distribution at depth in central New York State. Eos Trans. AGU, 63, 1118.
[6] Plumb, R. A., & Hickman, S. H. (1985). Stress-induced borehole elongation: A comparison between the four-arm dipmeter and the borehole televiewer in the Auburn geothermal well. Journal of Geophysical Research: Solid Earth, 90(B7), 5513-5521. https://doi.org/10.1029/JB090iB07p05513
[7] Zoback, M. D., Moos, D., Mastin, L., & Anderson, R. N. (1985). Well bore breakouts and in situ stress. Journal of Geophysical Research: Solid Earth, 90(B7), 5523-5530. https://doi.org/10.1029/JB090iB07p05523
[8] Zheng, Z., Kemeny, J., & Cook, N. G. (1989). Analysis of borehole breakouts. Journal of Geophysical Research: Solid Earth, 94(B6), 7171-7182. https://doi.org/10.1029/JB094iB06p07171
[9] Mastin, L. G., “An analysis of stress-induced elongation of boreholes at depth,” M.S. thesis, Stanford Univ., Stanford, California, USA, 1984.
[10] Barton, C. A., Zoback, M. D., & Burns, K. L. (1988). In-situ stress orientation and magnitude at the Fenton Geothermal Site, New Mexico, determined from wellbore breakouts. Geophysical Research Letters, 15(5), 467-470. https://doi.org/10.1029/GL015i005p00467
[11] Tingay, M., Reinecker, J., & Müller, B. (2008). Borehole breakout and drilling-induced fracture analysis from image logs. World Stress Map Project, 1-8.
[12] Karadeniz, K.E., and Ozturk, H. (2019). Estimation of Horizontal Principal Stress Orientation Using FMI Log for a Mining Project. In The 26th International Mining Congress and Exhibition of Turkey. Antalya: UCTEA Chamber of Mining Engineers.
[13] Kirsch, C. (1898). Die theorie der elastizitat und die bedurfnisse der festigkeitslehre. Zeitschrift des Vereines Deutscher Ingenieure, 42, 797-807.
[14] Jaeger, J. C., & Cook, N. G. (2014). W. 1979. Fundamentals of Rock Mechanics. Chapman and Hall, London, 593.
[15] Zoback, M. D. (2010). Reservoir geomechanics. Cambridge University Press.
[16] Shen, B. (2008). Borehole breakouts and in situ stresses. SHIRMS, 1, 407-418.
[17] Atkinson, B. K. (1984). Subcritical crack growth in geological materials. Journal of Geophysical Research: Solid Earth, 89(B6), 4077-4114. https://doi.org/10.1029/JB089iB06p04077

Kutay E. KARADENİZ is a M.Sc. student at Mining Engineering Department of Middle East Technical University (METU). He gained his B.Sc. from the same department and university. His major field of studies are rock mechanics and numerical modelling.
Hasan OZTURK is a Professor at Mining Engineering Department of Middle East Technical University (METU). He gained his B.Sc. and M.Sc. from the same university. He got his Ph.D. from University of Alberta. His major field of studies are rock mechanics and numerical modelling.